INTERMEDIATE LEVEL LAGRANGIAN SUBSURFACE MEASUREMENTS IN THE NORTHEAST PACIFIC: ISOBARIC RAFOS FLOAT DATA

Tetyana Margolina, Curtis A. Collins, Thomas A. Rago, Robert G. Paquette[1]

Department of Oceanography, Naval Postgraduate School, Monterey, California, USA (tmargoli@nps.edu; collins@nps.edu; tarago@nps.edu)

Newell Garfield

Romberg Tiburon Center, San Francisco State University, San Francisco, California, USA (garfield@sfsu.edu)

An edited version of this paper was published by AGU.

Citation: Margolina, T., Collins, C. A., Rago, T. A., Paquette R. G., and N. Garfield (2006), Intermediate level Lagrangian subsurface measurements in the northeast Pacific: Isobaric RAFOS float data, *Geochem. Geophys. Geosyst.*, *7*, Q09002, doi:10.1029/2006GC001295.

To view the published open abstract, go to http://dx.doi.org and enter the DOI: 10.1029/2006GC001295.

[1] Deceased May 8, 2005

Abstract

Isobaric RAFOS floats have been used to track the California Undercurrent and to investigate its continuity since 1992. The data include 61 quasi-Lagrangian subsurface trajectories sampled for the most part between 150 and 600 m. The data set allow estimates of Eulerian and Lagrangian statistics for the region, studies of mesoscale eddy activity, and analysis of seasonal variability of circulation patterns off Central California. A browsable web-based inventory and a Graphical User Interface have been developed to provide access to this data set including interactive manipulation of the data.

Index Terms: 4223 Oceanography: General: Descriptive and Regional oceanography;
4516 Oceanography: Physical: Eastern boundary currents;
4520 Oceanography: Physical: Eddies and mesoscale processes

Keywords: California Undercurrent; RAFOS isobaric floats, mesoscale eddies.

1. Introduction

Although the California Undercurrent (CU) is one of the most observed and studied of the Eastern boundary undercurrents, several basic dynamic and kinematic issues remain unresolved: its continuity in both space and time [*Pierce et al.*, 2000], its role in onshore-offshore exchange processes [*Garfield et al.*, 1999], and, since it provides a direct path from the tropics to subpolar regions, its role in transporting properties between oceanic gyres [*Castro et al*., 2001]. Lagrangian measurements using subsurface RAFOS floats were undertaken to address these questions.

Deployment of RAFOS floats in the CU began in 1992 [among others, see *Collins et al.*, 1996, 2003, 2004; *Garfield et al.*, 1999, 2001]. An extensive data set of 61 subsurface trajectories of isobaric RAFOS floats now exists. This paper presents an overview of the RAFOS data collection and provides a Graphical User Interface (GUI) application for RAFOS float data visualization and analysis. Its purpose is to make the data easily accessible and available for community use.

The paper is organized as follows: section 2 describes observational techniques, including broadcast schedules, deployment depths and temporal coverage of the data, as well as a description of the RAFOS floats as quasi-isobaric surface followers; section 3 contains a brief overview of experimental results, including charts of trajectories, means and variance ellipses, eddy statistics and an animation of results; and the final section presents the application for access and manipulation of the data set.

2. Observational Techniques

RAFOS floats [*Rossby et al.*, 1986] are manufactured from glass tubes about 1.5 m long by 0.1 m in diameter. A satellite antenna, thermistor, electronics and batteries are inserted into the glass tube, which is then closed using an aluminum end plate with a hydrophone mounted on the outside. A port through the end plate provides a conduit for *in situ* pressure measurement. All the floats were isobaric and ballasted to float on a given pressure surface (350 dbar in 1992–1993; 275, 290 and 350 dbar in 1994; 300 dbar in 1995; and 275 dbar since 1996). Floats 3 to 62 were ballasted at the Deep Ocean Simulation Facility, Naval Civil Engineering Laboratory, Port Hueneme, California, by NPS, while subsequent floats were ballasted at Woods Hole Oceanographic Institution by the manufacturer, Sea Scan, Inc. After launch, the float recorded both the time of arrival (TOA) of acoustic signals from moored sound sources and the ambient pressure and temperature. The length of the subsurface mission was determined prior to launch and was limited by battery capacity and computer memory. At the end of the mission, after releasing its ballast, the float surfaced and relayed its stored data to shore via the ARGOS data collection system on the NOAA POES satellites. While broadcasting at the surface, the floats were tracked by satellite.

Although the floats are expendable, five were found, recovered and returned to NPS. Four (NPS#41, 64, 83 and 87) were reconditioned and sent on second mission as NPS#94, 75, 98 and 105, respectively. The mission of NPS#75 was successful; NPS #94 was due up September 17, 2003, but never broadcast; NPS #98 is still on its mission, and NPS#105 surfaced on schedule on September 30, 2005, and is currently broadcasting.

2.1. Sound Source Array

The acoustic sound source array is shown in Figure 1. Table 1 includes the positions of the sources with their broadcast schedules. With the exception of a Hydro-Acoustic Low Frequency HLF-5 series and a "Rossby" sound source deployed at Hoke Seamount in 1999 and 2004, respectively, the sound sources were manufactured by Webb Research, Inc. The sources broadcast a low-frequency acoustic signal, an 80-s FM pulse centered near 260 Hz, which increased linearly 1.523 Hz from start (259.375 Hz) to end (260.898 Hz). The sound sources were moored near the mean depth of the axis of the deep sound channel, which ranges from 500 to 600 m off the California Coast [*Johnson and Norris*, 1968]. The sound source array ensonified coastal waters from Northern Mexico to Vancouver Island, although some near-shore regions, particularly in the Southern California bight, were shadowed by coastal islands. Four NPS sound sources (SS1–4) were initially deployed in August 1992, signaled three times per day. These sources were moored standard SOFAR floats. They were replaced in August 1994 with three sources that signaled twice per day. The source offshore from Pt. Arena, SS4, was eliminated in 1994 due to floats' erratic signal reception (possibly reflections or reverberations from the nearby slope and shadowing by Pt. Arena). In addition to the NPS sound sources, NOAA Pacific Marine Environmental Laboratory (PMEL) moored a sound source to calibrate an acoustic earthquake monitoring array. The PMEL source (V1) was installed in May 1993 near the Juan de Fuca Ridge. A second PMEL source (V2) was installed in February 1998 at Thompson Seamount.

Originally, the NPS sources broadcast three times a day, one after the other at half-hour intervals. Then the NPS transmitting schedule was changed to twice per day. Now, the broadcasting sequence begins with PMEL source, continues with the NPS sources and is finished by the Hoke source. More details on sound source location, broadcast schedule and performance are given in Table 1.

The sound sources were monitored at the NPS Pt. Sur Ocean Acoustic Observatory [*Orcutt et al.*, 2000]. The standard deviations, after linear trends were removed, for recorded arrival times over a two-year period for sources SS1, SS2, and SS3 were 0.167, 0.162, and 0.183 s, respectively. This indicates that the sources were stable and that timing errors due to different ray paths were small [*Garfield et al.*, 1999].

In May and June of 1994, five floats (21, 22, 24, 30, and 27 – the last did not collect any usable data) were deployed within a Coastal Tomography Array to verify tomography measurements. These floats were each operational for a twenty-three days, sampling of 21 or 24 times daily. The data from these floats provided high-frequency Lagrangian measurements that were used to examine errors of RAFOS navigation [*Benson*, 1995].

2.2 Quasi-Lagrangian and quasi-isobaric.

An ideal isobaric float would settle to the specified pressure surface and remain at that pressure for the duration of its mission. However, the density of the RAFOS float depends in part upon the thermal expansion of the glass and end cap, and changes with the temperature of ambient ocean waters such that the float does not stay on an isobaric surface. *Goodman and Levine* [1990] derived a "response ratio" to quantify how well a float follows either isobaric (response ratio of one) or isopycnal (response ratio of zero)

surfaces. The response ratio for the NPS floats varied between 0.75 and 0.8. Most of the variation of the response ratio came from changes in the normalized buoyancy frequency. The mean (median) standard deviation of the pressure along the float trajectory was 26 (17) dbar for all mid-depth floats. A float will sink or shoal depending on the difference between its density and the ambient density of seawater by an amount determined by the vertical gradients of temperature and salinity at the float [*Swift and Riser*, 1994]. The quasi-isobaric nature of the RAFOS float makes it possible to reconstruct salinity changes along the float trajectory using RAFOS temperature and pressure records and CTD measurements of water characteristics at the launch point, provided there is no large change in the pressure of the float. CTD data for the launch position is available for 36 floats (Table 2).

A second reason that floats deviated from isobaric surfaces was that seawater leaked into the glass hull. A one gram change in float mass translates to approximately 40 dbar pressure change at intermediate depths. Leaking was especially problematic for floats 1 to 61. These floats carried the original design for closure, whereby the seal between the endplate and the glass tube depended primarily on the smoothness of the two surfaces. Upon closure, the glass tube was partially evacuated, and the pressure difference between inside and outside the tube (along with a shrinkable casing over the juncture) maintained the seal. Mostly, especially with the increased outside pressure after deployment, this worked. However, some floats did leak. Those that did exhibited one of two modes, dubbed “slow” and “fast”. Of 58 floats of this type that were deployed by NPS, there were 7 each of slow and fast sinkers (14 total). Starting with NPS#62, a new closure design using an “O”-ring to seal the joint between the end plate and glass tube appears to have stopped the leaking.

The RAFOS floats presented here are more isobaric than isopycnal, and therefore do not follow vertical movements of a water parcel. *Davis* [1983] shows that oceanic observations of quasi-Lagrangian floats provide a useful and direct description of lateral advection and eddy dispersion. As suggested by *Davis* [1991], the trajectories have been used as space- and time-averaging current meters and estimates of diffusivity were obtained from their quasi-Lagrangian character [e.g. *Garfield et al.*, 1999; *Collins et al.*, 2004].

2.3 Navigation

The distance between a float and a sound source was calculated using the measured TOA and the speed of sound, which was assumed to be constant at 1481 m/s throughout the processing. A float position was calculated by triangulation from the location of the sound sources and the distances to the float [*Paquette*, 1995].

The uncertainty of the final solution of the float trajectory may arise from several sources. [See *Benson*, 1995, for an error analysis.] The main systematic errors causing the inaccuracy of the float trajectory are variations of sound speed and clock drift. The value of sound speed used in the processing procedure was considered to be an average at the axis of the SOFAR channel in the California Current region (*Johnson and Norris,* 1968). Taking into consideration the variations of sound speed with temperature, salinity and pressure for the region under consideration, the difference between the true and assumed mean speeds was O(1–4 m/s), resulting in a possible position error of 0.25 km at 200 km.

The clock drifts are known only for those floats and sound sources which were recovered. For example, for three sound sources recovered after completion of the

Tomography Demonstration Experiment [*Benson*, 1995], the source clock drifts were determined as 0.622, 2.233, and –1.1 ms/day. Available estimates of float clock drifts are ± 0.03 s/day. Typical clock drift at an operational RAFOS board connected to a hydrophone at the Point Sur (California) Underwater Acoustic Observatory was about 0.06605 s/day. These relatively small clock drifts are insignificant for short-term missions, but could be a factor for longer missions. During data processing, a single correction was made to the source clocks to account for both unknown sound speed and clock drift [*Paquette*, 1995]. After applying this correction, the absolute uncertainty in position was estimated to be less than 10 km, with the short-term relative error for each float being generally about 1 km [*Garfield et al.*, 1999].

It is also important to estimate short-term quasi-random errors, which cause errors in high-frequency float motion. These are errors due to multi-path sound propagation, the resolution of the float correlator, and ambient noise. The errors caused by multi-path (fluctuations in sound signal phase and amplitude at a RAFOS float, signal distortion, etc.) and ambient noise (for example, from ship traffic) are difficult to estimate with any certainty. The correlator has an inherent minimum error of about ± 0.3 sec. This translates to an error of about 0.5 km in range.

The position accuracy is defined by the physical geometry of the sound sources in the array and the location of a float with respect to the sound source array. This is referred to as dilution of precision (DOP). DOP is a multiplier for other errors. The DOP links the accuracy of the range information from each source to the accuracy of the final navigational solution.

Two other induced processing errors which can significantly affect the accuracy of the float trajectory are temporal gaps between launch/first fix and last subsurface

fix/first ARGOS fix. The former may result in ~0.5 km error for a mean current of 10 cm/sec. The latter, whose time interval can range from 3 to 6 hours, may result in as great as a 3 km distance for that same mean current of 10 cm/s.

In September 2004, the accuracy and precision of RAFOS tracking was studied in the region off Central California using a sea glider equipped with a hydrophone and a RAFOS processor (http://iop.apl.washington.edu/seaglider/). Position errors were estimated through comparison of RAFOS trilaterated positions with mean positions of the seaglider estimated by dead reckoning from surface GPS fixes using depth-averaged current within a dive (J. Gobat, personal communication, 2005). Uncorrected range error for a sound speed of 1480 m/s varied from 0.8 to 18.4 km (the mean error was ~ 9 km) for different sound sources and glider-source distances. After sound speed and clock drift corrections, the rms position error was 2.4 km.

2.4 Temperature and Pressure measurements

In addition to recording the TOA of the acoustic signals from the moored sound sources used for float navigation, the floats also recorded temperature and pressure. Temperature and pressure were measured over a 1-s averaging time interval after each listening cycle, which, depending on the mission parameters, meant one to three samples daily. The RAFOS floats prior to #62 measured temperature with accuracy of 0.2ºC uncalibrated, 0.1ºC calibrated against a resistance substitution box, with resolution of 0.005ºC. The accuracy of pressure measurements was about 14 db. Seascan DLD-2 floats (NPS#62 and late) measured pressure with accuracy of 2.8 db or better, and temperature (0 to 32ºC) with resolution (accuracy) of 0.001°C (0.01ºC).

Throughout the region, temperature (salinity) typically decreases (increases) with pressure. Temperature recorded by the float varies inversely with pressure. This is due to the quasi-isobaric nature of the float: effects of thermal expansion result in the float sinking when temperature increases. This behavior is particularly useful when the float is in shallow water and moving slowly as it confirms that the float has not grounded.

2.5. Experimental design.

Table 2 contains information on all successful RAFOS float missions, where "successful" means the float yielded a subsurface trajectory. The floats were sorted by launch date. Table 2 also provides basic information on launch sites, target depths, surfacing time/location, and float performance (i.e. mean and standard deviation of pressure and temperature along the float trajectory, and mission duration). The deployment schedule is given in Figure 2.

The sampling plan was generally to launch triads of RAFOS floats over the continental slope on cruises of opportunity. Adjacent floats in these triads were less than 20 km apart. Between July 1993 and December 2001, 14 triads were deployed, the last of which surfaced in March 2004. Launch sites are shown in Figure 3. The three primary launch locations were: west of San Francisco, off Monterey Bay and south of Point Sur.

The initial effort was focused on launching floats that would pass through an array of current meter moorings to the north of Pt. Arena [*Chereskin et al.*, 2000]. Beginning in February 1997, floats were launched along isobaths to the south of Point Sur to try to document regions of submesoscale vortex formation. After November 1999 intermediate-depth floats were launched to the west of Monterey Bay and Point Sur in conjunction with regional hydrographic surveys. Although the launch times for the floats

were not evenly distributed throughout a year, each season had nearly the same number of observations (Figure 4).

The first two floats were short 30-day missions to check system operation. Mission lengths were then increased, first to 60 days, then longer (Figure 2). Floats with shorter missions listened to sound sources two or three times daily, floats with longer missions once daily or every other day (Table 2).

3. Results

The experiment started in 1992, with first floats surfacing the same year. Numerous papers have been published analyzing the trajectories of floats that have completed their mission [*Collins et al.,* 1996, 2003, 2004; *Garfield et al.,* 1999, 2001; *Orcutt et al.,* 2000].

An animation (Figure 5) traces 15-day trajectory segments of the mid-depth floats. These trajectories exhibit three patterns (Figure 6): poleward flow in the California Undercurrent; reversing flow near the continental margin; and westward migration [*Garfield et al.*, 1999]. The westward migration of the floats was often accompanied by anticyclonic eddy-like motion (see Figure 7). Forty five "loopers" were visually identified. Each consisted of two or more consecutive loops with almost 80% moving westward at about 1.9 cm/s. Table 3 summarizes characteristics of anticyclonically looping segments of float trajectories. There was a large diversity in eddy radii and periods. Further discussion of loopers will be published in a separate paper.

Along the coast, the mean speed of the floats as well as principle axis of variance was alongshore (Figure 8). Between Point Conception and Cape Mendocino the magnitude of the mean velocity was 4 ± 1 cm/s with the mean flow vector oriented

toward 329 ± 17º and the principle axis of variance directed toward 337 ± 12º. These results are in good agreement with those obtained by *Garfield et al.* [1999, 2001].

Garfield et al. [1999] pointed out an important mechanism for floats to enter the ocean interior from the undercurrent as formation of submesoscale coherent vortices (SCVs), which they referred to as California Undercurrent (CU) eddies or "cuddies". Although the dynamical effect of these cuddies on the CU is unclear, they are able to transport CU waters a long distance into the interior of the subtropical gyre. *Lukas and Santiago-Mandujano* [2001] observed a cuddy at the ALOHA time series site north of Oahu, Hawaii.

In the work of *Collins et al.* [2003] the seasonal variability of the kinetic energy and eddy field in the California Current System was estimated from the RAFOS floats deployed over 1998-2002. It was shown that the kinetic energy of the CU had two pronounced extrema in late spring and early fall, while the eddy field was especially intense in autumn. The same data set was used by *Collins et al.* [2004] to estimate the seasonal variability of the CU in three large geographical boxes that spanned the length of central and northern California and were located successively farther offshore. It was shown that the California Undercurrent occurred year-round in the coastal and transition zones which extended to 190 km offshore. Three different dispersive regimes of float motion were identified depending on how the particle dispersion increases with time: ballistic transport (quadratic growth), normal diffusion (linear growth), and anomalous westward sub-diffusion, the last induced by Rossby wave-like structures..

When calculating statistics from these data, one should keep in mind that estimates will be biased by array design [*Garfield et al.,* 1999; *Garfield et al.,* 2001]. The

alongshore and across-shore diffusivities were 580 and 230 m^2/s, respectively, for the Undercurrent region between Point Conception and Cape Mendocino.

4. GUI

To provide access to the RAFOS data and allow visualization and interactive manipulation of the data, we have provided a suite of graphical user interfaces with the following capabilities:

- easy access to the searchable database;
- visualization of either all available, or an acquired subset of, RAFOS trajectories;
- the ability to track float movement and retrieve the associated pressure and temperature information;
- computation of Eulerian statistics (mean velocity and variance ellipse) for a cluster of trajectories within a customized rectangular region.

The GUI created in MATLAB 6.5 is available at http://www.oc.nps.navy.mil/npsRAFOS/. It is possible to run the GUI in MATLAB or as a stand-alone application.

The process of data loading takes no more than 30 s for a Pentium 4 CPU, during which time the GUI is non-interactive. Two main modes are possible using this GUI: 1) visualization of a single float trajectory (Figure 9b) or (2) drawing of all or parts of trajectories during some predefined time period (Figure 9a). Visualization of pressure and temperature along float trajectories is available for both the single and group modes, as illustrated in Figure 9b-c. The last panel of the last diagram (Figure 9d) demonstrates the process of calculating and visualizing mean velocities and ellipses of variance [*Freeland*

et al., 1975; *Davis*, 1991]. Eulerian statistics for all the trajectory fragments in a chosen region are re-calculated with a one-day time step. Because of the "accumulating" nature of this process, the beginning visualization should be considered as very approximate due to low statistical significance.

Acknowledgements

Elements of the observational program have been supported by the Office of Naval Research, the Oceanographer of the Navy, the Naval Oceanographic Office, the National Science Foundation, the National Oceanic and Atmospheric Administration, and the Naval Postgraduate School. Dr. Everett Carter helped initiate the program. The officers and crews of *R/V Point Sur, R/V New Horizon*, and *R/V Wecoma* helped deploy sources and floats. TM was supported as a NATO Postdoctoral Fellow by the National Science Foundation. Drs. Leonid Ivanov and Oleg Melnichenko have contributed to the authors' understanding of Lagrangian statistics and their application to ocean dynamics. We also wish to thank Professor Thomas Rossby and an anonymous reviewer for their close reading of the manuscript and insightful comments, which helped improve this paper.

References

Benson, K. (1995), High frequency subsurface Lagrangian measurements in the California current with RAFOS floats, M.S. thesis, 88 pp., Naval Postgraduate School, Monterey, Calif. http://www.oc.nps.navy.mil/npsRAFOS/BENSONthesisPDF.pdf

Castro, C. G., F. P. Chavez, and C. A. Collins (2001), The role of the California Undercurrent in the export of denitrified waters from the eastern tropical North Pacific, *Global Biogeochem. Cycles*, *15*(4), 819–831, doi:10.1029/2000GB001324.

Chereskin, T. K., M. Y. Morris, P. P. Niiler, P. M. Kosro, R. L. Smith, S. R. Ramp, C. A. Collins, and D. L. Musgrave (2000), Spatial and temporal characteristics of the mesoscale circulation of the California Current from eddy-resolving moored and shipboard measurements, *J. Geophys. Res.*, *105*(C1), 1245–1269.

Collins, C. A., N. Garfield, R. Paquette, and E. Carter (1996), Lagrangian measurement of subsurface poleward flow between 38ºN and 43ºN along the West Coast of the United States during Summer 1993, *Geophys. Res. Lett.*, *23*(18), 2561–2564.

Collins, C. A., L. M. Ivanov, and O. V. Melnichenko (2003), Seasonal Variability of the California Undercurrent: Statistical Analysis based on the Trajectories of Floats with Neutral Buoyancy, *Phys. Oceanogr.*, *13*(3), 135–147.

Collins, C. A., L. M. Ivanov, O. V. Melnichenko, and N. Garfield (2004), California Undercurrent variability and eddy transport estimated from RAFOS float observations, *J. Geophys. Res.*, *109*, C05028, doi:10.1029/2003JC002191.

Davis, R. E. (1983), Oceanic property transport, Lagrangian particle statistics, and their prediction, *J. Mar. Res.*, *41*, 163–194.

Davis, R. E. (1991), Observing the general circulation with floats, *Deep Sea Res.*, *38*(Suppl. 1), S531–S571.

Freeland, H. J., P. B. Rhines, and T. Rossby (1975), Statistical observations of the trajetories of neutrally buoyant floats in the North Atlantic, *J. Mar. Res.*, *33*, 383–404.

Garfield, N., C. A. Collins, R. G. Paquette, and E. Carter (1999), Lagrangian Exploration of the California Undercurrent, 1992–1995, *J. Phys. Oceanogr.*, *29*, 560–583.

Garfield, N., M. Maltrud, C. A. Collins, T. A. Rago, and R. G. Paquette (2001), Lagrangian Flow in the California Undercurrent, an Observation and Model Comparison, *J. Mar. Syst.*, *29*, 201–220.

Goodman, L., and E. R., Levine (1990), Vertical motion of neutrally buoyant floats, *J. Atmos. Oceanic Technol.*, *7*, 38–49.

Johnson, R. H., and R. A. Norris (1968), Geographic variation of SOFAR speed and axis depth in the Pacific Ocean, *J. Geophys. Res.*, *73*, 135–141.

Lukas, R., and F. Santiago-Mandujano (2001), Extreme water mass anomaly observed in the Hawaii Ocean Time-series, *Geophys. Res. Lett.*, *28*(15), 2931–2934.

Orcutt, J., C. deGroot-Helin, W. Hodgkiss, W. Kuperman, W. Munk, F. Vernon, P. Worcester, E. Bernard, R. Dziak, C. Fox, C.-S. Chiu, C. Collins, J. Mercer, R. Odom, M. Park, D. Soukur, and R. Spindel (2000), Long-term Observations in Acoustics — the Ocean Acoustic Observatory Federation, *Oceanography*, *13*(2), 57–63.

Paquette, R.G. (1995), RAFOS Float Manual, 44 pp., Naval Postgraduate School, Monterey, Calif. (Available from Department of Oceanography, Naval Postgraduate School, 833 Dyer Rd., RM Sp328, Monterey, CA 93943).

Pierce, S. D., R. L. Smith, P. M. Kosro, J. A. Barth, and C. D. Wilson (2000), Continuity of the poleward undercurrent along the eastern boundary of the mid-latitude Pacific, *Deep Sea Res.*, *47*, 811–829.

Rossby, T., D. Dorson, and J. Fontaine (1986), The RAFOS System, *J. Atmos. Oceanic Technol.*, *3*, 672–679.

Swift, D. D., and S. C. Riser (1994), RAFOS Floats: Defining and targeting surfaces of neutral buoyancy, *J. Atmos. Oceanic Technol.*, *11*, 1079–1092.

Figure Captions

Figure 1. Study region showing locations of sound sources. White contours represent 200, 1000, 2000, 3000, and 4000 m isobaths.

Figure 2. Deployment schedule.

Figure 3. Launch sites.

Figure 4. Frequency distributions of number of float launches (upper panel) and float daily observations (lower panel) by month.

Figure 5. Animation tracing 15-day trajectory segments of the mid-depth floats.

Figure 6. Spaghetti diagram of RAFOS float trajectories. Three trajectories patterns — poleward flow in the CU, reversing flow near the continental margin, and westward migration — are exhibited.

Figure 7. Anticyclonic (left) and cyclonic (right) loopers. Red dots show where a float was entrained by an eddy.

Figure 8. Eulerian mean velocity and variance ellipses for the RAFOS floats. The box size is about one degree for both latitude and longitude. The units of the colorbar are cm/s and present the actual sizes of the principal axes of standard deviation. Numbers in the center of each ellipse are the number of measurements inside a corresponding box.

Figure 9. GUI diagrams: (a) spaghetti diagram; visualization of pressure (b) and temperature (c) along a single float trajectory; (d) diagram of mean velocities and ellipses of variance.

Table 1. Sound Sources

Source	Latitude, N	Longitude, W	Instrument Depth, m	Water Depth, m	Broadcast (UTC)	Launched	Recovered	Comments
SS1	34.2958°	124.0969°		3012	0030 0830 1630	21 June 1992 @ 1555 UTC		
							24 May 1994 @ 2030 UTC	Clock was 1.5862 sec slow at recovery
	34.2993º	124.1026º	605	3040	0430 1630	24 May 1994 @ 1730 UTC		
SS1b	33.0294º	120.9961º		558	0430	23 October 2002 @1736 UTC		
SS2	40.4612º	126.3895º		1704	0100 0900 1700	11 June 1992 @ 1614 UTC		
							3 June 1994 @ 1640 UTC	Clock was about 1 sec slow at recovery
	40.4138º	126.3853º			0500 1700		3 June 1994 @ 1531 UTC	
SS2b	43.9165º	126.3988º	566	3019	0500 1700	16 October 2001 @0410 UTC		
SS3	37.0117º	127.5350º		4752	0130 0930 1730	9 August 1992 @ 0505 UTC		
							20 August 1994 @ 0415 UTC	clock was about 1 second slow at recovery
	37.1092º	127.5350º		4752	0530 1730	20 August 1994 @ 0222 UTC		
							8 May 2000 @ 1752 UTC	clock was about 9 seconds slow at recovery
	37.1094º	127.5773º		4751.19	0530 1730	May 2000 @ 2303 UTC		
SS4	38.5854º	123.9091º		1980	0200 1000 1800	12 June 1992 @ 1613 UTC		

						20 May 1993 @ 2145 UTC	clock was about 2 seconds slow at recovery
	38.5852º	123.9086º	1980	0200 1000 1800	21 May 1993 @ 0115 UTC		
						5 June 1994 @ 0130 UTC	clock was about 17 seconds slow at recovery
V1	45.9400º	130.0340º		0400 1600	16 August 1993		*(PMEL equipment)*
V2	46.0310º	128.6288º	1430	0400 1600	14 February 1998		
Hoke	32.1057º	126.9103º	780	0600	2 May 1999 @ 2000 UT		Scripps Tomography Source (HLF5)
						5 May 2000 @ 1657 UTC	clock was within a second of correct at recovery
	32.1058º	126.9104º	785	0600 1800	5 May 2000 @ 2114 UT		
						7 November 2001 @ 1505 UTC	source went to sleep after 10 pings. (Operator error)
	32.1062º	126.9080º	796	0600	8 October 2001 @ 2114 UT		
						25 October 2002 @ 1919 UTC	
	32.1062º	126.9097º	768	0600	25 October 2002 @ 2053 UT		Slider Source
						8 October 2004	
	32.1062º	126.9097º	768	0600	8 October 2004		Rossby Source

Table 2. Float Information

Float ID	Launch							Surface		Sampling rate, per day	RAFOS performance		Mission, days	
	Date	φ^oN / λ^oW	Water depth, m	Temperature, ºC		Pressure, dbar	Salinity, (CTD)	Date	φ^oN / λ^oW		Planned pressure, dbar	Actual pressure and temperature	Planned	Actual
				CTD	RAFOS									
NPS#1	12-Aug-1992	37.1986 123.2753	1881[1]		4.911	635.7		11-Sep-1992	36.7380 122.3490	3	350	688.6 ± 19.0 4.58 ± 0.12	30	30
NPS#2		37.8025 123.4859	1835[1]		4.954	622.2		11-Sep-1992	37.7363 123.5183	3	350	637.3 ± 9.1 4.97 ± 0.08	30	30
NPS#3	07-Jul-1993	37.7733 123.5489	2350		6.934	302.5		05-Sep-1993	37.7140 123.6760	3	350	361.7 ± 15.9 6.79 ± 0.13	60	60
NPS#5		37.7798 123.4548	1690		8.369	141.6		05-Sep-1993	42.7260 125.1070	3	350	140.1 ± 14.8 7.95 ± 0.17	60	60
NPS#7		37.8396 123.5124	1780		6.994	291.8		05-Sep-1993	36.8517 126.4800	3	350	325.4 ± 20.7 6.88 ± 0.12	60	60
NPS#4	03-Sep-1993	37.8389 123.5125	1797		8.926	231.0		01-Jan-1994	38.6470 130.2750	2 every other day	350	252.1 ± 12.8 7.49 ± 0.37	120	120
NPS#8		37.7820 123.4561	1733		7.570	313.9		30-Dec-1993	42.3190 126.8890	2 every other day	350	292.2 ± 19.3 6.91 ± 0.30	120	119
NPS#10		37.7723 123.5483	2400		7.337	292.8		01-Jan-1994	38.2680 125.9080	2 every other day	350	305.8 ± 11.0 6.84 ± 0.17	120	120

[1] from http://topex.ucsd.edu/cgi-bin/get_data.cgi

NPS#6	20-Nov-1993	37.8408 123.5122	1833[1]	7.0402	7.117	332.1	34.1629	02-Mar-1994	37.7090 124.9042	3 every other day	350	387.2 ± 17.5 6.40 ± 0.19	101	101
NPS#11		37.7822 123.5614	2475	7.3482	6.949	302.3	34.0564	02-Mar-1994	37.5560 125.3660	3 every other day	350	321.6 ± 7.5 7.18 ± 0.13	101	101
NPS#13		37.7821 123.4568	1660	8.1666	7.479	279.9	34.1267	02-Mar-1994	37.7610 124.5590	3 every other day	350	286.9 ± 5.8 7.40 ± 0.07	101	101
NPS#9	11-Jan-1994	37.7735 123.5485	2400		6.466	282.4		23-Apr-1994	40.3140 125.2180	3 every other day	350	527.4 ± 54.8 4.53 ± 0.46	101	101
NPS#12		37.8398 123.5153	1750		7.462	312.4		23-Apr-1994	36.3660 122.8890	3 every other day	350	399.8 ± 28.7 6.41 ± 0.27	101	101
NPS#14		37.7810 123.4563	1950		7.684			23-Apr-1994	38.4630 124.9890	3 every other day	350	170.4 ± 12.3 7.33 ± 0.13	101	101
NPS#19	25-Apr-1994	37.6177 123.1092	800	6.0701	6.190	428.9	34.1946	11-Nov-1994	42.4420 126.9330	1	275	462.7 ± 41.2 5.67 ± 0.44	203	201
NPS#24	17-May-1994	36.3377 123.0207	3495[1]	5.2172	5.622	552.5	34.2336	09-Jun-1994	37.4880 123.8720	24	275	547.5 ± 4.6 5.62 ± 0.04	23	23
NPS#30	18-May-1994	36.4997 123.0012	3093[1]	6.9589	7.759	289	34.0875	10-Jun-1994	37.4720 124.3130	21	275	288.6 ± 4.9 7.60 ± 0.11	23	23
NPS#21	19-May-1994	36.5912 122.5894	2541[1]	6.1960	6.631	355	34.1115	10-Jun-1994	38.3450 124.0970	24	275	363.4 ± 9.4 6.65 ± 0.12	23	23
NPS#22	19-May-1994	36.5210 122.8083	2995[1]	5.0829	5.713	580.5	34.2574	10-Jun-1994	37.6610 124.1570	21	275	577.4 ± 4.4 5.60 ± 0.05	23	23

[1] from http://topex.ucsd.edu/cgi-bin/get_data.cgi

NPS#28	12-Aug-1994	37.6199 123.1120	800	7.093	7.188	351.2	34.1477	19-Dec-1994	42.0740 126.2720	2	350	361.0 ± 9.2 6.87 ± 0.24	130	130
NPS#33		37.5898 123.1778	1220	5.1553	5.208	653.5	34.2742	30-May-1995	37.3480 123.8670	1	350	655.6 ± 8.6 5.13 ± 0.12	499	293
NPS#26	22-Aug-1994	37.0879 123.0166	1000	7.7544	7.902	313.2	34.1193	30-Dec-1994	39.5860 125.8720	2	290	314.5 ± 9.6 7.51 ± 0.13	130	130
NPS#31		37.4744 124.5254	4050	6.1361	6.646	349.3	3.0878	30-Dec-1994	38.0320 127.1430	2	290	370.8 ± 11.1 6.96 ± 0.14	130	130
NPS#29	25-Oct-1995	35.9763 121.7635	1070	7.000	7.082	371.6	34.1204	28-Jun-1996	32.9530 127.1280	2	300	450.3 ± 14.7 5.64 ± 0.94	260	249
NPS#32	07-Aug-1995	37.4488 123.1827	943		7.433			06-Oct-1996	37.8990 132.8940	1	300	318.8 ± 78.2 7.24 ± 0.68	499	427
NPS#35		37.3729 123.2048	1070		7.969			05-Nov-1996	35.7940 133.4070	1	300	315.0 ± 75.3 7.28 ± 0.41	499	457
NPS#42	25-Jul-1996	36.3339 122.2533	980		7.001			12-May-1997	35.8410 125.4140	1	275	456.7–637.4 5.17 ± 0.48	292	292
NPS#39	29-Jul-1996	36.8341 122.3669	1090	6.4444	6.659	481.4	34.1659	10-Dec-1997	52.4960 160.9340	1	275	503.3 ± 26.8 5.75 ± 0.46	499	458
NPS#41		36.7841 122.2679	810	7.0229	6.995	442.7	34.2183	17-Nov-1997	41.8050 127.8490	1	275	430.6–1021 4.55 ± 0.60	499	476
NPS#46		36.8830 122.3296	590	7.1415	7.550	402.2	34.2105	19-Sep-1997	45.2160 126.2380	1	275	394.6–849.9 4.84 ± 0.62	499	415

NPS#43	25-Feb-1997	36.1070 121.8836	1000	6.5352	6.540	381.4	34.1534	13-Dec-1997	36.3820 130.8370	1	275	416.3 ± 14.3 6.68 ± 0.16	292	292
NPS#51		36.1315 121.8407	720	6.6836	6.310	409.7	34.1813	08-Jul-1998	33.3450 137.0710	1	275	193.2–465.3 7.22 ± 0.96	499	464
NPS#48	29-Aug-1996	36.3365 122.1755	800		7.227			10-Jan-1998	58.7220 138.0260	1	275	315.06 ± 45.0 6.48 ± 0.27	499	499
NPS#49		36.5114 122.0923	1020		8.474			23-Mar-1997	36.5670 122.1500	1	275	402.37 ± 62.5 7.14 ± 0.55	499	207
NPS#50		36.4248 122.1752	900		7.114			09-Jan-1998	46.1200 125.5590	1	275	179–404.3 7.21 ± 0.46	499	499
NPS#53	11-Sep-1997	37.0843 123.1097	1770		7.067			22-Apr-1998	37.9040 127.8060	2	275	—	224	224
NPS#55		37.0980 123.0843	1340					22-Apr-1998	39.5040 128.1900	2	275	368.2 ± 6.4 6.17 ± 0.12	224	224
NPS#62	29-Apr-1998	35.4133 121.5879	1063		6.384			25-Jun-1999	34.6100 124.5650	2	275	375.7 ± 28.5 6.42 ± 0.20	422	422
NPS#64		36.0005 122.0062	1281		6.026			25-Jun-1999	47.7290 126.1640	2	275	381.5 ± 10.1 5.85 ± 0.29	422	422
NPS#65		34.4480 120.9249	810		6.949			24-Jun-1999	33.0480 129.1610	2	275	359.2 ± 12.4 6.76 ± 0.08	422	422
NPS#63	17-May-1998	34.6933 121.6867	1382					12-Jul-1999	32.2230 126.8590	2	275	363.0 ± 19.1 6.79 ± 0.18	422	422

NPS#66	27-Oct-1998	36.0102 121.8342	1188		6.414			23-Dec-1999	36.7290 125.1590	2	275	405.0 ± 9.5 6.37 ± 0.20	422	422
NPS#67		35.8323 121.7494	1009		6.451			23-Dec-1999	39.1270 124.8520	2	275	390.9 ± 18.8 6.15 ± 0.36	422	422
NPS#68		35.9177 121.7898	1024		6.152			23-Dec-1999	33.8290 122.6780	2	275	419.2 ± 21.7 6.13 ± 0.13	422	422
NPS#69	05-May-1999	35.0190 123.8652	4184	5.0640	5.038	608.4	34.2771	18-May-2000	36.4400 125.1790	2	275	660.6 ± 47.9 4.95 ± 0.10	380	380
NPS#71		35.1419 123.7222	4112	5.1035	5.129	568.5	34.2583	18-May-2000	43.3380 125.1530	2	275	613.8 ± 41.2 5.02 ± 0.15	380	380
NPS#72	21-Nov-1999	36.0478 122.0244	1320	5.0229	4.963	668.1	34.3295	12-Feb-2001	39.6770 129.0820	2	275	722.1 ± 28.5 4.63 ± 0.19	450	450
NPS#73		35.9660 122.2056	1715	7.3739	7.298	287.2	34.1332	12-Feb-2001	34.5410 131.5740	2	275	313.0 ± 17.0 7.89 ± 0.27	450	450
NPS#75		35.8838 122.3849	3105	8.1397	8.090	210.7	34.0923	12-Feb-2001	34.5880 130.4560	2	275	128.1 ± 44.6 9.96 ± 1.20	450	450
NPS#80	26-Jul-2000	36.6321 122.4799	2541	8.1685	8.112	311.5	34.1776 34.1755	23-Sep-2001	35.6310 125.1280	2	275	348.0 ± 53.4 7.31 ± 0.40	425	425
NPS#81		36.4605 122.8013	3031	7.6450	7.609	240.6	34.0496 34.0470	22-May-2002	39.6650 126.9140	1	275	275.8 ± 53.7 7.54 ± 0.20	666	666
NPS#82		36.5488 122.6156	3034	8.0543	8.120	258.3	34.1736 34.1718	24-Sep-2001	42.0240 130.1310	2	275	215.5 ± 22.6 7.61 ± 0.25	425	425

NPS#83	11-Sep-2000	35.9674 122.1988	1687	7.5507	7.455	241.2	34.0548 34.0525	29-Dec-2001	42.2210 127.8180	2	275	250.0 ± 49.5 7.70 ± 0.28	475	475
NPS#84		35.8887 122.3661	3142	5.9111	5.898	449.6	34.1708 34.1688	09-Jul-2002	37.3700 126.6940	1	275	457.4 ± 20.3 5.85 ± 0.18	667	667
NPS#85		36.0560 122.0027	1306	8.9185	8.807	137.5	33.9454 33.9419	09-Jul-2002	40.3000 131.9210	1	275	134.4 ± 38.2 8.72 ± 0.39	667	667
NPS#87	20-May-2001	36.4818 122.7850	2998	6.6769	6.772	335.9	34.1369 34.1407	06-Nov-2002	38.9450 124.5640	2	275	348.4 ± 11.8 6.22 ± 0.39	500	535
NPS#88		36.5342 122.6043	2804	7.0506	6.873	323.1	34.1444 34.1451	28-Jul-2003	43.8250 126.9850	1	275	397.7 ± 64.3 5.71 ± 0.46	800	800
NPS#89		36.3835 122.9591	3305	6.6530	6.553	325.8	34.0788 34.0793	28-Jul-2003	43.4220 126.1490	1	275	333.5 ± 11.9 6.36 ± 0.25	800	800
NPS#90	06-Dec-2001	36.4894 123.5087	3593	7.1528	7.154	293.5	34.1000 34.0861	09-Mar-2004	48.2570 126.5970	1	275	304.4 ± 15.1 6.86 ± 0.28	825	825
NPS#91	05-Dec-2001	36.5877 123.3475	3469	7.0324	6.758	310.9	34.0991 34.0852	09-Mar-2004	38.3470 133.5670	1	275	344.5 ± 18.0 6.49 ± 0.16	825	825
NPS#92	05-Dec-2001	36.6655 123.1342	3259	7.1266	7.111	282.9	34.0836 34.0703	09-Mar-2004	39.4680 128.2140	1	275	294.4 ± 13.3 6.56 ± 0.28	825	825

Table 3. Characteristics of anticyclonic looping trajectories

Float ID	Start			Mean depth, dbar	Mean temperature, ºC	Number of loops	Period, days	Swirl velocity cm/s	Diameter, km	EKE, cm^2/s^2	Translation velocity, cm/s	Direction, º	*Ro*
	Date mm/dd/year	Latitude ºN	Longitude ºW										
NPS#5	8/17/1993	42.17	125.35	148.4	7.8	2	7	19.6	37.7	191.6	0.8	134	0.11
NPS#6	1/3/1994	37.24	124.53	394.8	6.3	2	29	12.8	103.4	82.2	1.6	280	0.03
NPS#7	7/27/1993	37.18	125.04	340.8	6.9	5	7	19.8	38.1	195.8	2.9	283	0.12
NPS#8	10/17/1993	41.38	125.26	301.8	6.9	2	14	17.7	70.0	157.2	3.1	338	0.05
NPS#11	11/23/1993	37.73	123.88	322.1	7.2	8	12	11.7	39.9	68.8	1.7	255	0.07
NPS#13	11/26/1993	37.57	123.55	287.0	7.4	5	19	14.2	76.0	100.6	1.4	263	0.04
NPS#14	1/27/1994	37.92	124.55	—	7.3	4	21	9.5	54.2	45.1	1.1	296	0.04
NPS#19	6/30/1994	41.40	125.61	451.2	6.0	5	12	16.9	53.8	142.0	1.9	244	0.06
NPS#26	11/15/1994	39.00	124.48	319.8	7.6	4	11	10.1	30.1	50.8	4.0	288	0.07
NPS#28	10/28/1994	40.98	125.71	365.8	6.7	3	16	15.2	67.7	115.8	3.3	323	0.05
NPS#31	8/28/1994	38.00	125.27	372.4	7.0	5	25	21.0	141.6	220.9	1.7	250	0.03
NPS#33	12/9/1994	39.39	124.57	661.5	5.2	2	36	5.5	54.1	15.3	0.6	206	0.02
NPS#41	8/27/1996	37.55	124.10	735.1	4.9	3	64	11.6	203.4	67.5	0.9	255	0.01
NPS#39	7/3/1997	44.79	125.44	526.0	5.3	1.5	74	7.0	141.8	24.3	0.6	347	0.01
NPS#43	4/16/1997	37.02	123.85	416.2	6.7	2	22	17.9	100.5	161.4	3.7	221	0.04
NPS#43	6/6/1997	36.20	127.67	421.9	6.7	3	63	11.1	192.9	61	1.9	256	0.01
NPS#48	2/1/1997	44.55	124.47	346.9	6.4	2	17	7.2	33.9	26.2	2.2	339	0.04
NPS#51	6/14/1997	36.58	127.53	360.4	7.0	3	93	9.5	241.4	44.9	1.1	249	0.01
NPS#66	7/28/1999	37.33	123.38	404.8	6.8	2	13	9.9	35.4	49.1	1.1	112	0.06
NPS#66	8/30/1999	37.23	124.99	389.7	6.5	2	58	10.6	168.7	56.4	0.5	236	0.01
NPS#67	5/23/1999	40.64	125.77	389.6	5.8	5	5	20.0	25.3	191.7	7.2	256	0.16
NPS#67	6/18/1999	40.18	127.84	393.5	5.8	2	11	16.8	50.7	140.4	4.6	262	0.07
NPS#67	7/15/1999	40.45	129.34	400.7	5.9	7	13	15.4	55.3	118.3	0.2	241	0.06
NPS#69	8/23/1999	36.90	125.25	645.4	5.0	2	78	8.0	171.6	32.0	0.3	249	0.01
NPS#72	8/21/2000	40.77	126.76	737.5	4.5	2	48	7.5	98.9	28.0	2.8	249	0.02
NPS#73	12/13/1999	36.14	123.72	315.4	7.9	30	14	19.4	76.0	188.1	2.1	256	0.06
NPS#75	6/29/2000	38.57	126.61	118.2	10.2	2	25	15.2	103.4	115.4	2.4	217	0.03
NPS#83	10/22/2001	42.21	126.52	231.5	8.0	9	8	26.3	54.3	346.1	2.2	290	0.10
NPS#85	6/9/2001	42.99	127.79	130.8	8.6	4	11	16.2	49.0	131.2	0.7	264	0.07
NPS#88	12/19/2001	43.94	126.67	470.8	5.4	6	19	9.2	47.2	42.3	1.3	280	0.04
NPS#89	8/15/2001	40.66	124.83	323.0	6.7	5	5	13.6	17.3	93.1	2.3	333	0.17
NPS#89	9/26/2001	42.16	125.55	347.1	6.8	3	4	17.4	20.8	152.2	3.4	43	0.17
NPS#90	1/24/2002	38.54	125.93	309.3	7.2	2.5	28	14.3	108.9	102.7	2.2	320	0.03
NPS#90	11/5/2003	47.22	125.34	319.1	6.8	30	4	18.2	20.8	165.4	1.6	322	0.16
NPS#91	8/22/2002	40.60	129.50	349.4	6.7	3	29	9.3	74.9	43.1	3.2	279	0.03

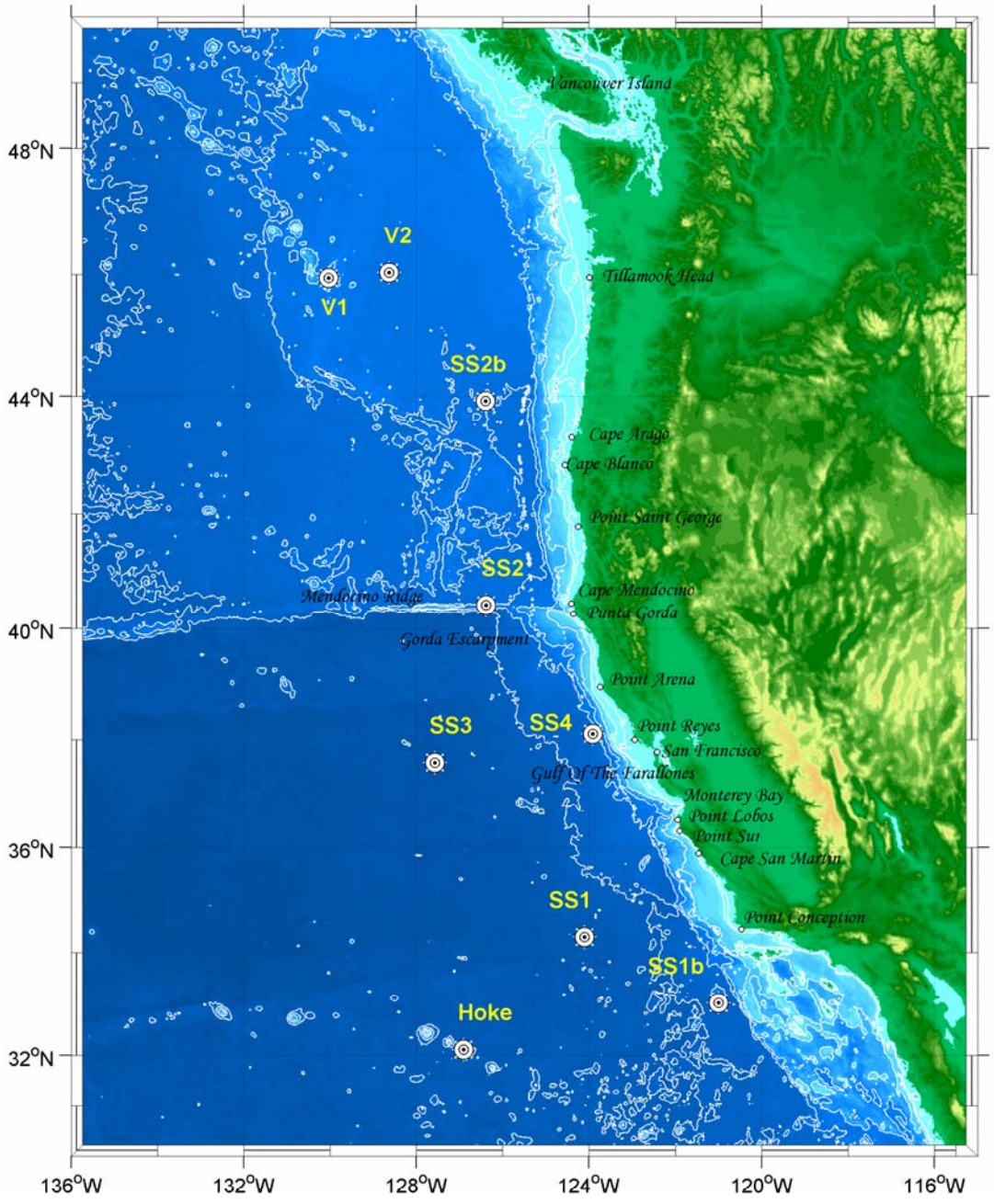

Figure 1. Study region showing locations of sound sources. White contours represent 200, 1000, 2000, 3000, and 4000 m isobaths.

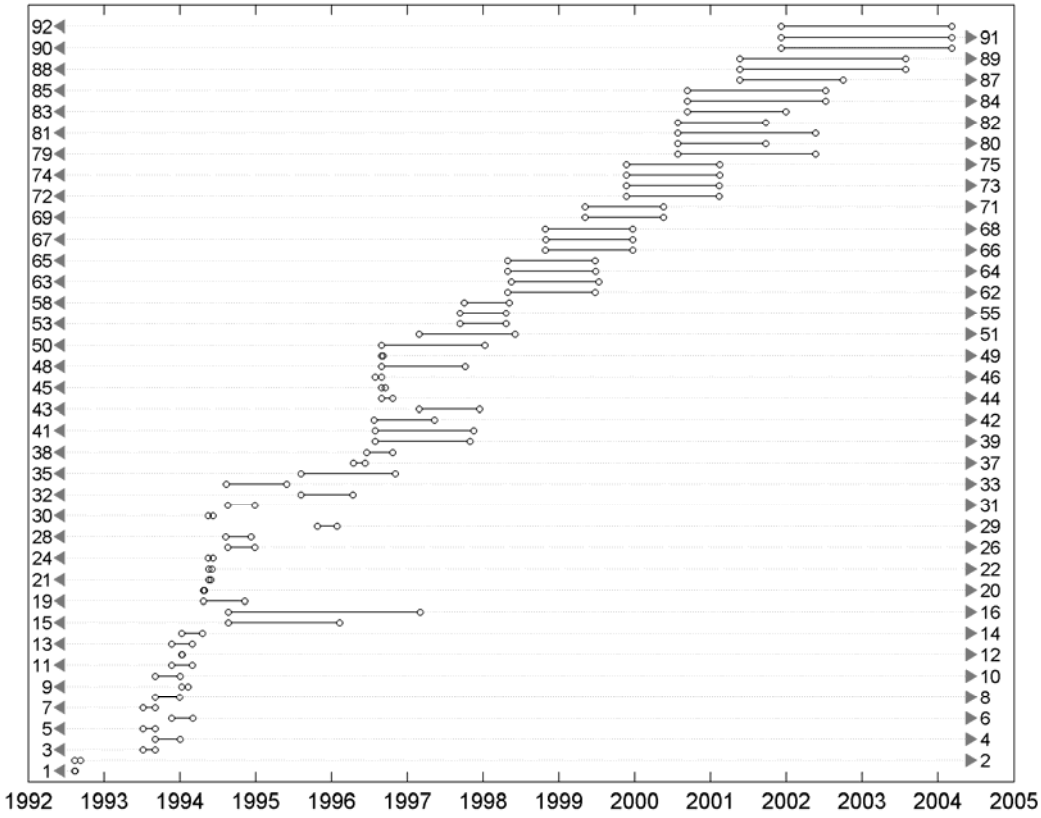

Figure 2. Deployment schedule.

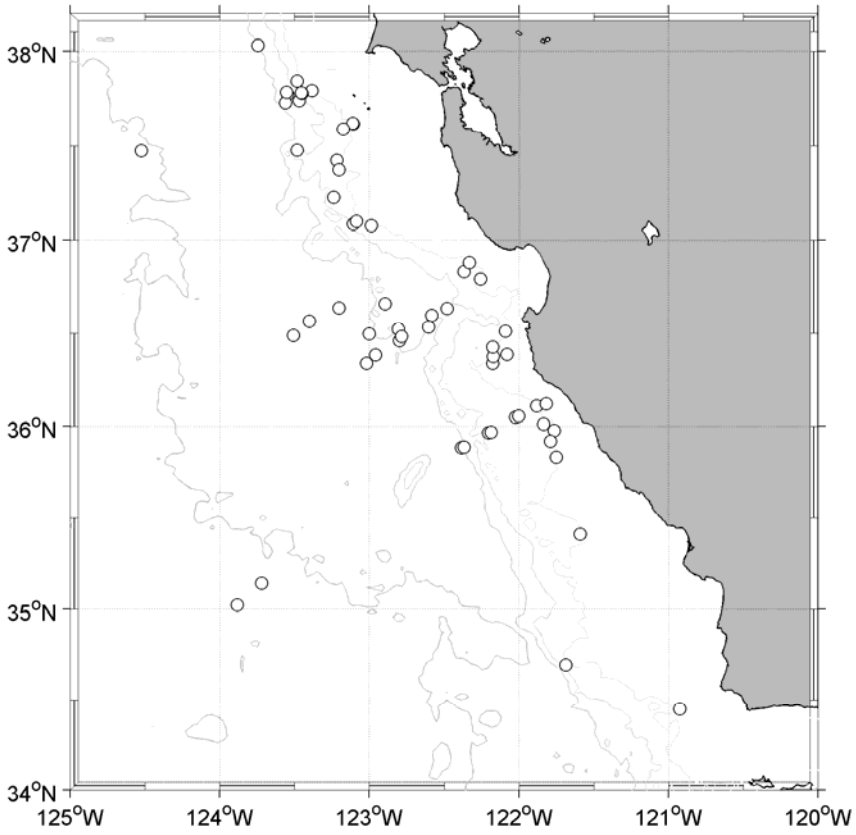

Figure 3. Launch sites.

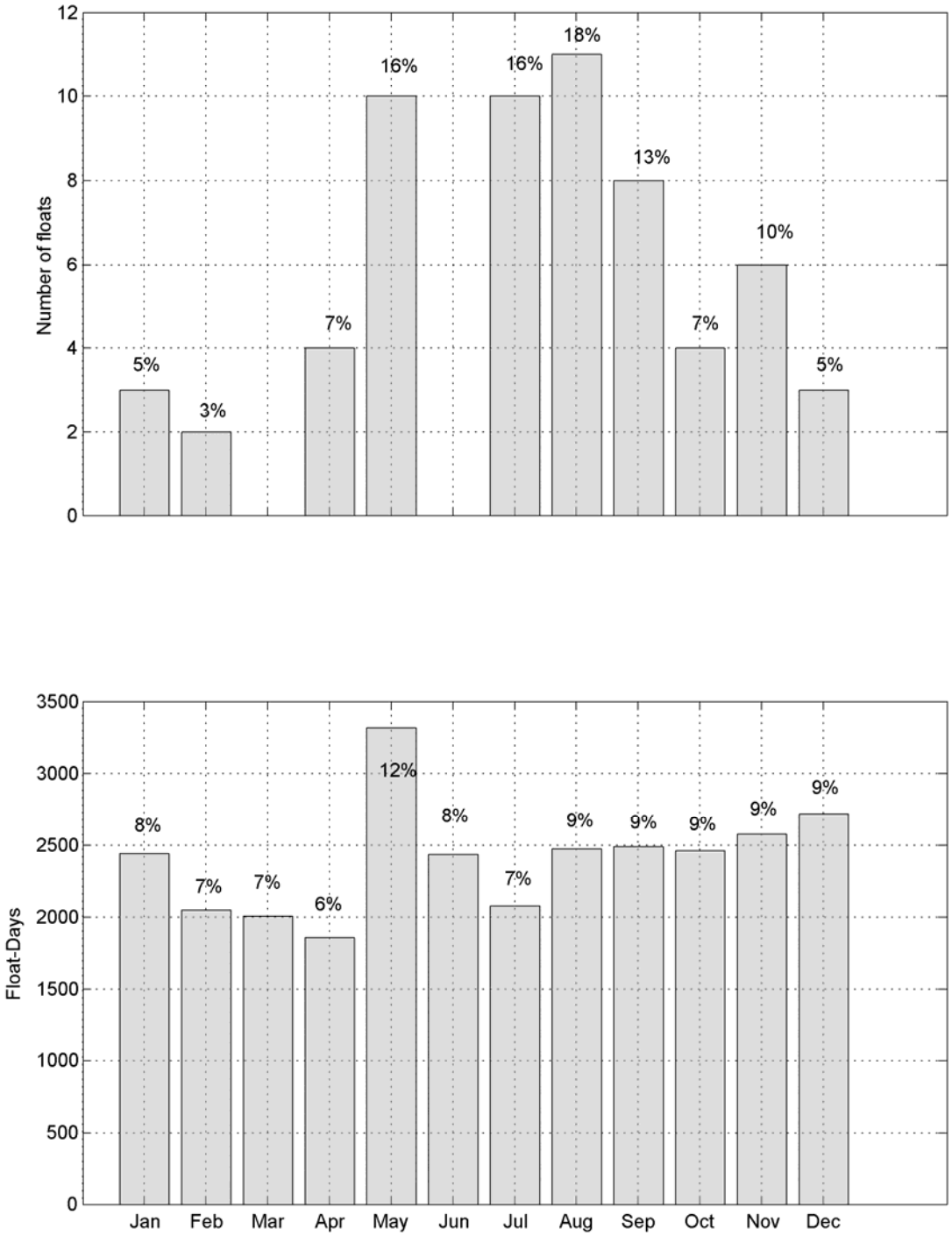

Figure 4. Frequency distributions of number of float launches (upper panel) and float daily observations (lower panel) by month.

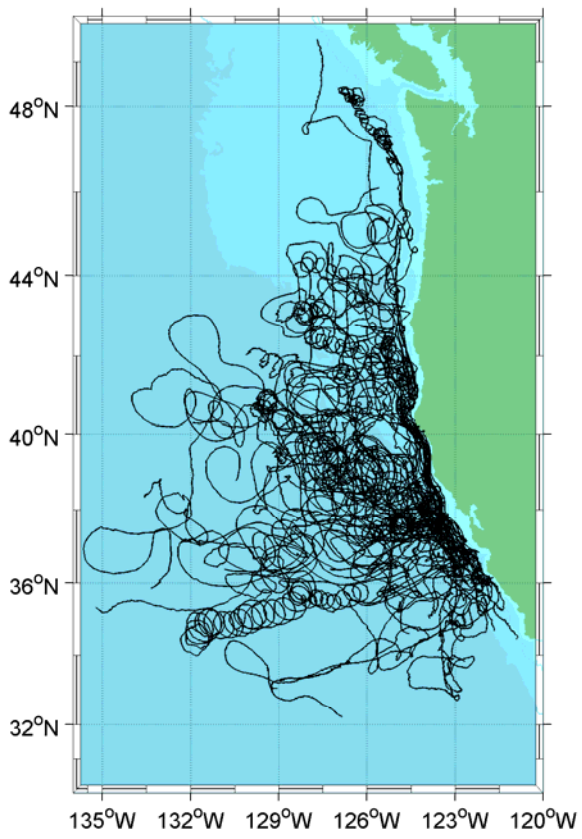

Figure 6. Spaghetti diagram of RAFOS float trajectories. Three trajectories patterns — poleward flow in the CU, reversing flow near the continental margin, and westward migration — are exhibited.

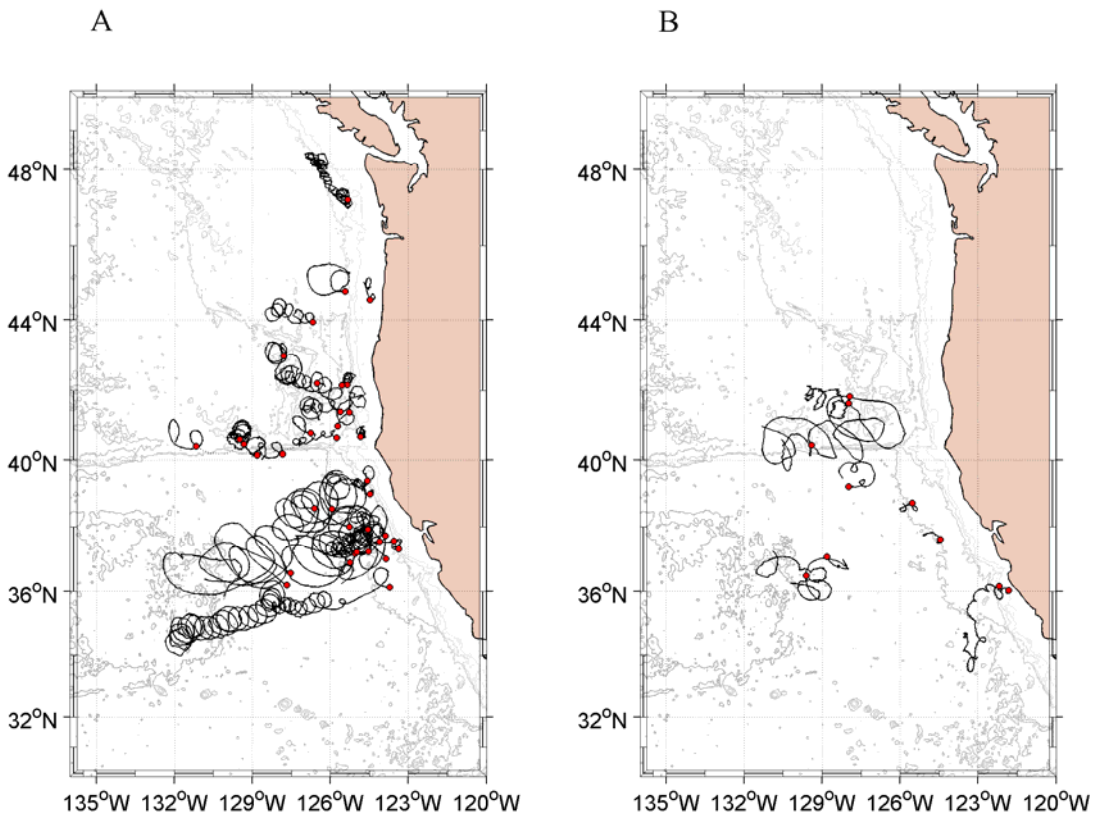

Figure 7. Anticyclonic (left) and cyclonic (right) loopers. Red dots show where a float was entrained by an eddy.

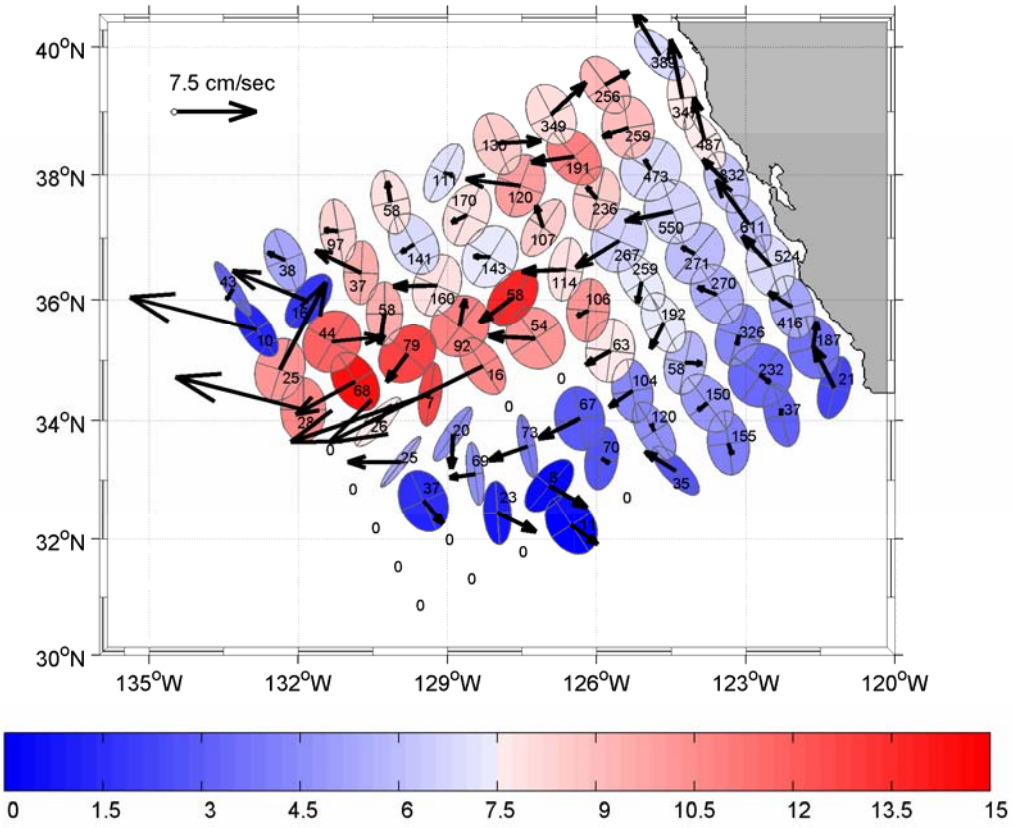

Figure 8. Eulerian mean velocity and variance ellipses for the RAFOS floats. The box size is about one degree for both latitude and longitude. The units of the colorbar are cm/s and present the actual sizes of the principal axes of standard deviation. Numbers in the center of each ellipse are the number of measurements inside a corresponding box.

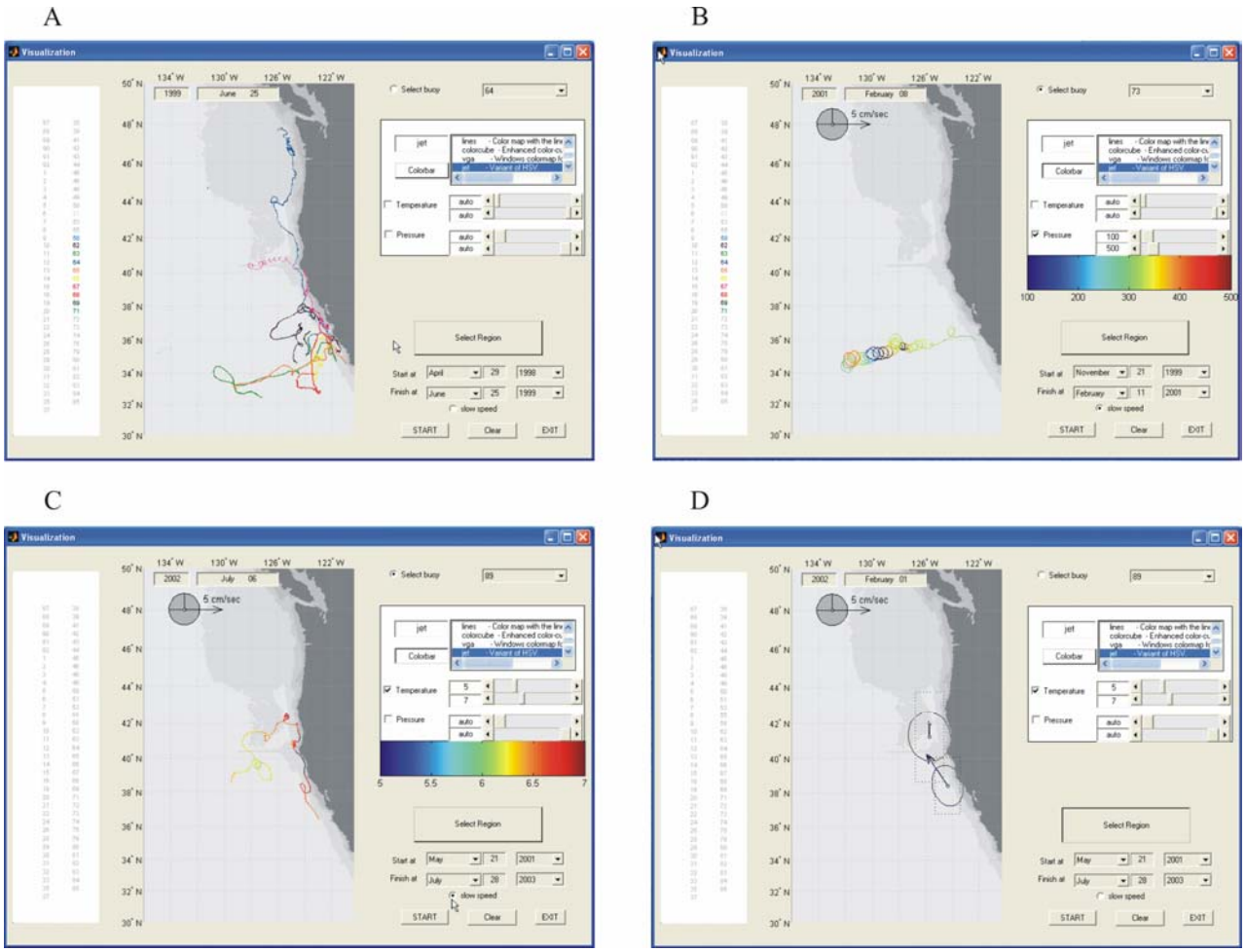

Figure 9. GUI diagrams: (a) spaghetti diagram; visualization of pressure (b) and temperature (c) along a single float trajectory; (d) diagram of mean velocities and ellipses of variance.